Cellular/Molecular

Phosphoinositide Modulation of Heteromeric Kv1 Channels Adjusts Output of Spiral Ganglion Neurons from Hearing Mice

Katie E. Smith,[1]* Lorcan Browne,[1,2]* David L. Selwood,[2] David McAlpine,[1] and Daniel J. Jagger[1]

[1]UCL Ear Institute, University College London, London WC1X 8EE, United Kingdom, and [2]Wolfson Institute for Biomedical Research, University College London, London WC1E 6BT, United Kingdom

Spiral ganglion neurons (SGNs) relay acoustic code from cochlear hair cells to the brainstem, and their stimulation enables electrical hearing via cochlear implants. Rapid adaptation, a mechanism that preserves temporal precision, and a prominent feature of auditory neurons, is regulated via dendrotoxin-sensitive low-threshold voltage-activated (LVA) K^+ channels. Here, we investigated the molecular physiology of LVA currents in SGNs cultured from mice following the onset of hearing (postnatal days 12–21). Kv1.1- and Kv1.2-specific toxins blocked the LVA currents in a comparable manner, suggesting that both subunits contribute to functional heteromeric channels. Confocal immunofluorescence in fixed cochlear sections localized both Kv1.1 and Kv1.2 subunits to specific neuronal microdomains, including the somatic membrane, juxtaparanodes, and the first heminode, which forms the spike initiation site of the auditory nerve. The spatial distribution of Kv1 immunofluorescence appeared mutually exclusive to that of Kv3.1b subunits, which mediate high-threshold voltage-activated currents. As Kv1.2-containing channels are positively modulated by membrane phosphoinositides, we investigated the influence of phosphatidylinositol-4,5-bisphosphate (PIP_2) availability on SGN electrophysiology. Reducing PIP_2 production using wortmannin, or sequestration of PIP_2 using a palmitoylated peptide (PIP_2-PP), slowed adaptation rate in SGN populations. PIP_2-PP specifically inhibited the LVA current in SGNs, an effect reduced by intracellular dialysis of a nonhydrolysable analog of PIP_2. PIP_2-PP also inhibited heterologously expressed Kv1.1/Kv1.2 channels, recapitulating its effect in SGNs. Collectively, the data identify Kv1.1/Kv1.2 heteromeric channels as key regulators of action potential initiation and propagation in the auditory nerve, and suggest that modulation of these channels by endogenous phosphoinositides provides local control of membrane excitability.

Key words: action potential; auditory; cochlea; excitability; Kv; PIP2

Significance Statement

Rapid spike adaptation is an important feature of auditory neurons that preserves temporal precision. In spiral ganglion neurons, the primary afferents in the cochlea, adaptation is regulated by heteromeric ion channels composed of Kv1.1 and Kv1.2 subunits. These subunits colocalize to common functional microdomains, such as juxtaparanodes and the somatic membrane. Activity of the heteromeric channels is controlled by cellular availability of PIP_2, a membrane phospholipid. This mechanism provides an intrinsic regulation of output from the auditory nerve, which could be targeted for therapeutic adjustment of hearing sensitivity.

Introduction

Spiral ganglion neurons (SGNs) are the first afferents of the mammalian auditory pathway, relaying acoustic information from cochlear hair cells to the brainstem. Each inner hair cell (IHC), the primary mechanoreceptors of the system, receives synaptic input from the peripheral neurites of 5–20 Type I SGNs (Nayagam et al., 2011), with the density of innervation maximal in the cochlear region with the highest sensitivity to sound (Meyer et al., 2009). Frequency tuning in individual SGNs is largely conferred by their location along the cochlea's tonotopic axis, with higher-frequency sounds coded toward the cochlear base (Liberman, 1982). IHCs respond to sound via a graded receptor potential triggering

Received Feb. 5, 2015; revised June 1, 2015; accepted June 24, 2015.

Author contributions: D.L.S., D.M., and D.J.J. designed research; K.E.S. and L.B. performed research; K.E.S., L.B., and D.J.J. analyzed data; K.E.S., L.B., and D.J.J. wrote the paper.

This work was supported by Action on Hearing Loss Grant P35021 to D.J.J. and D.M. and European Commission Grant 304912 to D.M., L.B. holds a UCL Crucible Studentship. We thank Jon Robbins (King's College London) for the kind gift of PIP_2-palpeptide and Martin Stocker (UCL) for the rKv1.1 and rKv1.2 cDNAs.

The authors declare no competing financial interests.

*K.E.S. and L.B. contributed equally to this work.

Correspondence should be addressed to Dr. Daniel J. Jagger, UCL Ear Institute, University College London, 332 Gray's Inn Road, London WC1X 8EE, United Kingdom. E-mail: d.jagger@ucl.ac.uk.

DOI:10.1523/JNEUROSCI.0496-15.2015

 0270-6474/15/3511221-12$15.00/0

Ca^{2+}-dependent glutamate release at the IHC-SGN synapse (Moser and Beutner, 2000). This activates large, but brief, AMPA receptor-mediated EPSCs within SGN boutons (Glowatzki and Fuchs, 2002). The resulting short-latency EPSPs almost always lead to the generation of phasic action potentials (APs) (Siegel, 1992; Rutherford et al., 2012), a rapidly adapting response enabling the auditory nerve to phase-lock reliably onto sound inputs, and ensuring high temporal fidelity (Rutherford et al., 2012).

In dissociated spiral ganglion cultures, where there is a lack of IHC synaptic input, SGNs display heterogeneous adaptive responses to maintained current injection (Mo and Davis, 1997; Lv et al., 2012). Although the relative distribution of adaptation rates differs between studies, a consistent observation is the predominance of very rapidly adapting (phasic firing) cells. The complement of voltage-gated ion channels expressed by the cultured neurons is proposed to regulate their intrinsic excitability (Liu et al., 2014). In cultures of neonatal mouse SGNs, rapid adaptation is regulated by dendrotoxin-sensitive, low-threshold voltage-activated (LVA) K^+ currents (Mo et al., 2002). The implication of a role for Kv1-family subunits has also been suggested in the auditory brain (Johnston et al., 2010). However, in SGNs cultured from adult guinea pigs, inhibition of LVA currents by dendrotoxin does not affect adaptation (Szabó et al., 2002), raising the possibility of developmental or interspecies differences in the contribution to the LVA current.

Here, we investigated the molecular physiology of the LVA currents and their association with rapid adaptation and excitability. In SGNs cultured from mice following the onset of hearing, sensitivity to subunit-specific toxins suggested that the LVA current is mediated via heteromeric assemblies of Kv1.1 and Kv1.2 subunits. Using confocal immunofluorescence, we localized Kv1.1 and Kv1.2 subunits together at specific subcellular domains, including the SGN somatic membrane, their axonal juxtaparanodes, and the first heminode located near the initial spike generator of the auditory nerve (Hossain et al., 2005). Finally, in agreement with observations in heterologous systems where Kv1.2 subunits are regulated by phosphoinositide signaling (Rodriguez-Menchaca et al., 2012; Kruse and Hille, 2013), the LVA current in SGNs was inhibited by depletion of phosphatidylinositol-4,5-bisphosphate (PIP_2), which had the effect of slowing adaptation. Our findings implicate Kv1.1/Kv1.2 heteromeric channels in the control of AP initiation and propagation in the cochlea, and identify them as novel therapeutic targets within the auditory nerve.

Materials and Methods

Animals. C56BL/6 mice were bred in an in-house facility and were killed by CO_2 inhalation followed by cervical dislocation. All animal work conformed to United Kingdom legislation outlined in the Animals (Scientific Procedures) Act 1986.

SGN culture. SGN cultures were prepared from the cochleae of P12-P21 mice of either sex. After death, the cochleae were removed and the modioli were isolated. The tissue was digested in 0.25% trypsin at 37°C for 30 min. Growth medium (DMEM containing 10% FCS, 10 mM HEPES, and 1% penicillin/streptomycin) was added, and the tissue was gently triturated. Cells were pelleted by gentle centrifugation (400 × *g*, 10 min), resuspended in growth medium, and plated onto glass coverslips pretreated with poly-L-lysine (50 μg/ml for 1 h). Coverslips were incubated in a humidified chamber at 37°C, 5% CO_2, for 1 h to allow the dissociated SGNs to adhere. Growth medium supplemented with 10 ng/ml BDNF was added, and the coverslips were returned to the incubator for 48–72 h.

SGN electrophysiology. Recordings were made from SGNs at room temperature (22°C–24°C), following 2–3 d *in vitro* (DIV). Glass coverslips were placed in a recording chamber mounted on an upright microscope (E600FN, Nikon). Recordings were performed in the whole-cell configuration using an Axopatch 200B patch-clamp amplifier (Molecular Devices) and a Digidata board (Molecular Devices) under the control of pClamp software (version 8, Molecular Devices). During recordings, cultures were superfused with artificial perilymph containing the following (in mM): 145 NaCl, 4 KCl, 1 $MgCl_2$, 1.3 $CaCl_2$, 10 HEPES, and 5 glucose, pH 7.3. Patch pipettes were pulled from capillary glass (GC120TF; Harvard Apparatus) using a vertical puller (Narishige). Pipettes had resistances of 2.8–4.5 MΩ when filled with the standard intracellular solution containing the following (in mM): 130 K-gluconate, 5 KCl, 2 MgATP, 2 Na_2ATP, 0.3 Na_3GTP, 10 Na_2-phosphocreatine, 1 EGTA, and 10 HEPES, pH 7.2. The liquid junction potential was measured as −13 mV and was subtracted off-line. Series resistance compensation was applied at 70%. Current-clamp and voltage-clamp protocols are described in Results and in the figure legends. Electrophysiological data were analyzed off-line using Clampfit (version 10, Molecular Devices) and Igor Pro (version 6.36, Wavemetrics). Voltage dependence of activation was calculated by fitting conductance-voltage data with the Boltzmann function, $G_{norm} = G_{min} + (G_{max} - G_{min})/(1 + \exp((V_{1/2} - V_m)/k))$, where G is conductance, $V_{1/2}$ is the half-maximal activation, V_m is the membrane potential, and k is the slope.

Drug stocks and application. Dendrotoxin-K (DTX-K), tityustoxin-Kα (TsTx), and κM-conotoxin RIIIJ (RIIIJ) were obtained from Alomone Labs. The three toxins were prepared as 50 or 100 μM stocks in water and stored at −20°C before dilution in artificial perilymph (100 nM) for patch-clamp recordings. Wortmannin (Santa Cruz Biotechnology) was prepared as a 1 mM stock in water and stored at −20°C before dilution to 100 nM or 10 μM in SGN growth medium. PIP_2-palpeptide (PIP_2-PP; a generous gift from Dr Jon Robbins, Kings College London) was supplied as a 10 mM stock solution in water and stored at −20°C in single-use aliquots before dilution in artificial perilymph (1 or 3 μM) for patch-clamp recordings. With the exception of wortmannin, which was preincubated with the SGN cultures for 1 h, toxins and peptides were applied through the bath perfusion system. For a subset of experiments, the standard intracellular solution was supplemented with diC_8PIP_2 (Echelon Bioscience). Working concentrations of 100 or 200 μM diC_8PIP_2 were prepared in standard intracellular solution and stored at −20°C before use.

Immunofluorescence. Whole cochleae from P20 C57BL/6 mice were fixed in 4% PFA in PBS for 40 min at room temperature. A small hole was made in the apex of the otic capsule allowing the PFA to perfuse into the cochlea. After fixation, the tissue was washed several times in PBS and the cochleae were decalcified in 4% EDTA for 48 h at 4°C. The otic capsules were mounted in 4% agarose and sectioned on a vibratome (1000 plus system, Intracel) at 200 μm intervals.

For antibody labeling, sections were permeabilized and blocked (0.2% Triton X-100 and 10% normal goat serum in PBS) for 40 min at room temperature. To reduce background fluorescence when using mouse monoclonal antibodies, sections were incubated for 1.5 h in Mouse Ig Blocking Reagent (Vector Laboratories). Primary antibodies were diluted 1:100 (Kv1.1, Kv1.2, Kv3.1b, PSD95, Pan Nav) or 1:1000 (β-tubulin antibody [TUJ1]) in blocking solution (0.1 M lysine and 0.1% Triton X-100 in PBS), and sections were incubated for 3.5 h at room temperature. After several washes in PBS, sections were incubated at room temperature for 1 h with AlexaFluor fluorescently labeled secondary antibodies (1:400 dilution in blocking solution; Invitrogen). Sections were washed several times in PBS and mounted in VECTASHIELD containing DAPI (Vector Laboratories).

Images were acquired using a confocal microscope (LSM510; Carl Zeiss) equipped with a 20× air objective (NA 0.75) and 63× water-immersion objective (NA 1.2). AlexaFluor-488, -555, and -633 fluorophores were excited using 488, 543, and 633 nm lasers, respectively, and emission was collected using 505–530 nm, 560–615 nm bandpass filters and a 650 nm long-pass filter, respectively. DAPI was excited using a 405 nm laser with emission collected using a 420–480 nm bandpass filter. Multichannel *z*-stacks were acquired using sequential scanning with a frame average of 4 and a *z*-step size of 2–2.3 μm (20×) or 1.4–1.8 μm

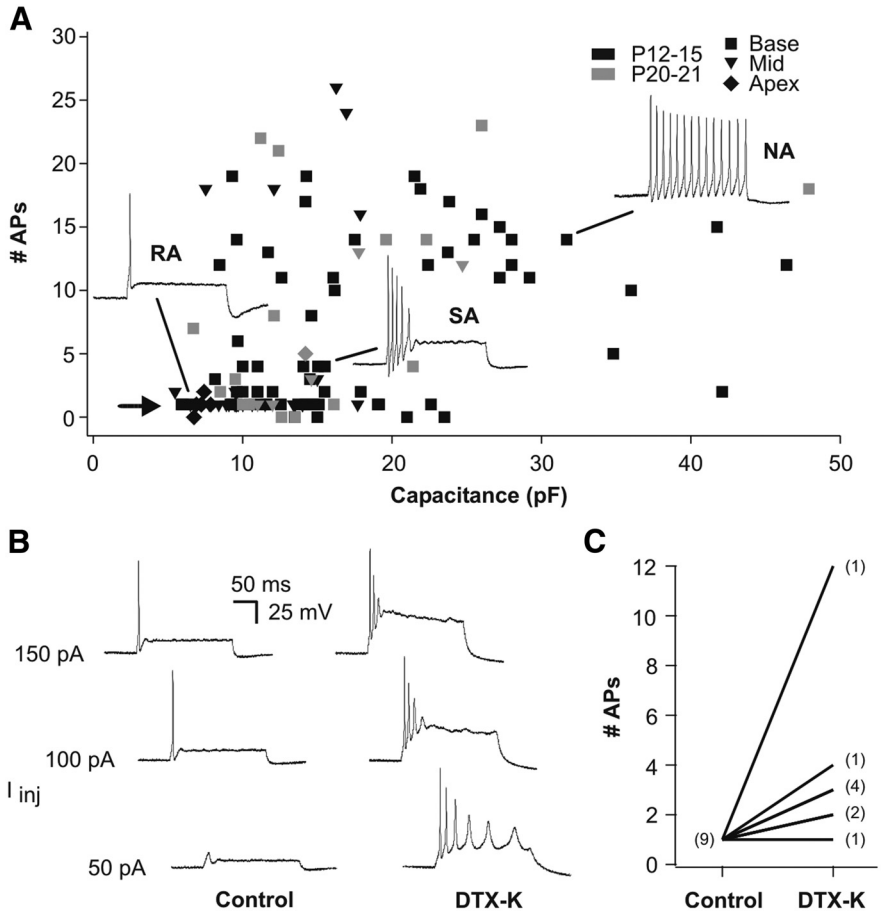

Figure 1. Heterogeneous excitability in populations of SGNs cultured from posthearing mice. ***A***, Scatter-plot of the number of action potentials (# APs) in response to a depolarizing current injection versus the recorded whole-cell membrane capacitance (C_m). The 200 ms current injections of 100 pA were applied from a holding potential of −73 mV. Arrow indicates the prominent subpopulation of rapidly adapting SGNs. Insets, Typical rapidly adapting (RA), slowly adapting (SA), and nonadapting (NA) SGNs from P12-P15 basal turn cultures. ***B***, Adaptation was slowed in RA neurons (P12-P15) following bath application of the Kv1.1-specific DTX-K (100 nM). Voltage responses to incremental 50 pA current injections from a holding potential of −73 mV are shown before (left) and after (right) the application of DTX-K. The current required to elicit AP firing was reduced following DTX-K exposure. ***C***, The number of APs elicited during a 100 pA current injection increased in 8 of 9 SGNs (P12-P15) following application of DTX-K. Numbers of recorded cells are indicated in parentheses.

(63×). Images shown are maximum intensity *z*-projections of 2–4 adjacent sections unless stated otherwise.

Antibodies. The mouse monoclonal neuronal Class III β-tubulin (subtype IgG_{2a}; clone TUJ1; Covance) was used as a neuronal marker. Mouse monoclonal antibodies for Kv1.1 (subtype IgG_1; clone K20/78), Kv1.2 (subtype IgG_{2b}; clone K14/16), Kv3.1b (subtype IgG_1; clone N16b/8), and PSD95 (subtype IgG_{2a}; clone K28/43) were obtained from the University of California Davis/National Institutes of Health NeuroMab Facility. Sodium channels were detected using a rabbit polyclonal Pan Nav antibody (Alomone Labs). Mouse monoclonal antibodies were detected by the application of the isotype-specific secondary antibodies, AlexaFluor-488goat anti-mouse IgG_{2b}, AlexaFluor-555 goat anti-mouse IgG_1, and AlexaFluor-633 goat anti-mouse IgG_{2a} (Invitrogen). AlexaFluor-633 goat anti-rabbit was used to detect the Pan Nav rabbit primary antibody.

Molecular biology. The rat cDNAs of Kv1.1 and Kv1.2 (kindly provided by Dr Martin Stocker, UCL), were cloned into pcDNA3 (Invitrogen) for heterologous expression in HEK293 cells: accession numbers: Kv1.1 (*Kcna1*), NM_173095; Kv1.2 (*Kcna2*), NM_012970. All constructs were verified by Sanger sequencing.

HEK293 cells. HEK293 cells were cultured in a humidified incubator at 37°C and 5% CO_2. Growth medium contained DMEM supplemented with 10% FCS, 2 mM L-glutamine, and penicillin/streptomycin (Invitrogen). At 1–2 d before transfection, cells were plated in 35 mm dishes to obtain a density of 70%–80%. Cells were transfected using 2.5 μg DNA and 5 μl Lipofectamine 2000 (Invitrogen). The transfection complex was incubated with the cells for 4 h in Opti-MEM media (Invitrogen) after which the transfection complex was replaced with normal growth medium. At ~22 h after transfection, cells were trypsinized and plated at low density onto glass coverslips. After a brief recovery (~3 h), coverslips were transferred into the recording chamber for voltage-clamp recordings. The conditions used for whole-cell patch clamp were as described for SGNs.

Results

Rapid adaptation in posthearing SGNs depends on Kv1.1/Kv1.2 heteromeric channels

In prehearing mice, the intrinsic excitability of cultured SGNs has been linked to their original location along the tonotopic axis of the cochlea (Adamson et al., 2002). To examine whether this relationship persists in SGNs from hearing mice, SGN cultures were prepared from apical, mid, and basal thirds of the cochlea from mice around the age of hearing onset (P12-P15) and 1 week after onset (P20-P21). The older age group was included to examine whether there were further maturational changes to SGN firing properties during the third postnatal week, as there is a recognized increase in hearing sensitivity during this period, as measured by decreasing thresholds for the compound action potential (Shnerson and Pujol, 1981). The excitability of SGNs from the two age groups, and originating from different cochlear turns (basal, mid, apical), was assessed by examining their response to a 200 ms depolarizing current injection (100 pA) from a holding potential of −73 mV (Fig. 1*A*). There was broad variability in individual responses to the stimuli, ranging from rapidly adapting (phasic firing) to nonadapting (tonic firing) behavior. Spontaneous APs were also observed in a number of cells in the absence of depolarizing stimuli. There was no clear relationship between adaptation behavior and somatic size (correlated with measured whole-cell membrane capacitance, C_m). SGNs from both age groups displayed these diverse firing properties, suggesting that heterogeneity of responses is established by hearing onset and maintained beyond. Despite this heterogeneity, however, a prominent subpopulation of rapidly adapting cells was apparent (Fig. 1*A*, arrow), and cells with these characteristics were the focus of the present study. The dissociated cultures used for the assessment of excitability properties in current-clamp mode, shown in Figure 1*A*, most likely included the small subpopulation of Type II SGNs, the afferent neurons of outer hair cells (Nayagam et al., 2011). However, these cells are readily distinguished from Type I SGNs in voltage-clamp mode (Jagger and Housley, 2003), enabling their removal from subsequent analyses. Consequently, the data reported here were obtained exclusively from Type I SGNs.

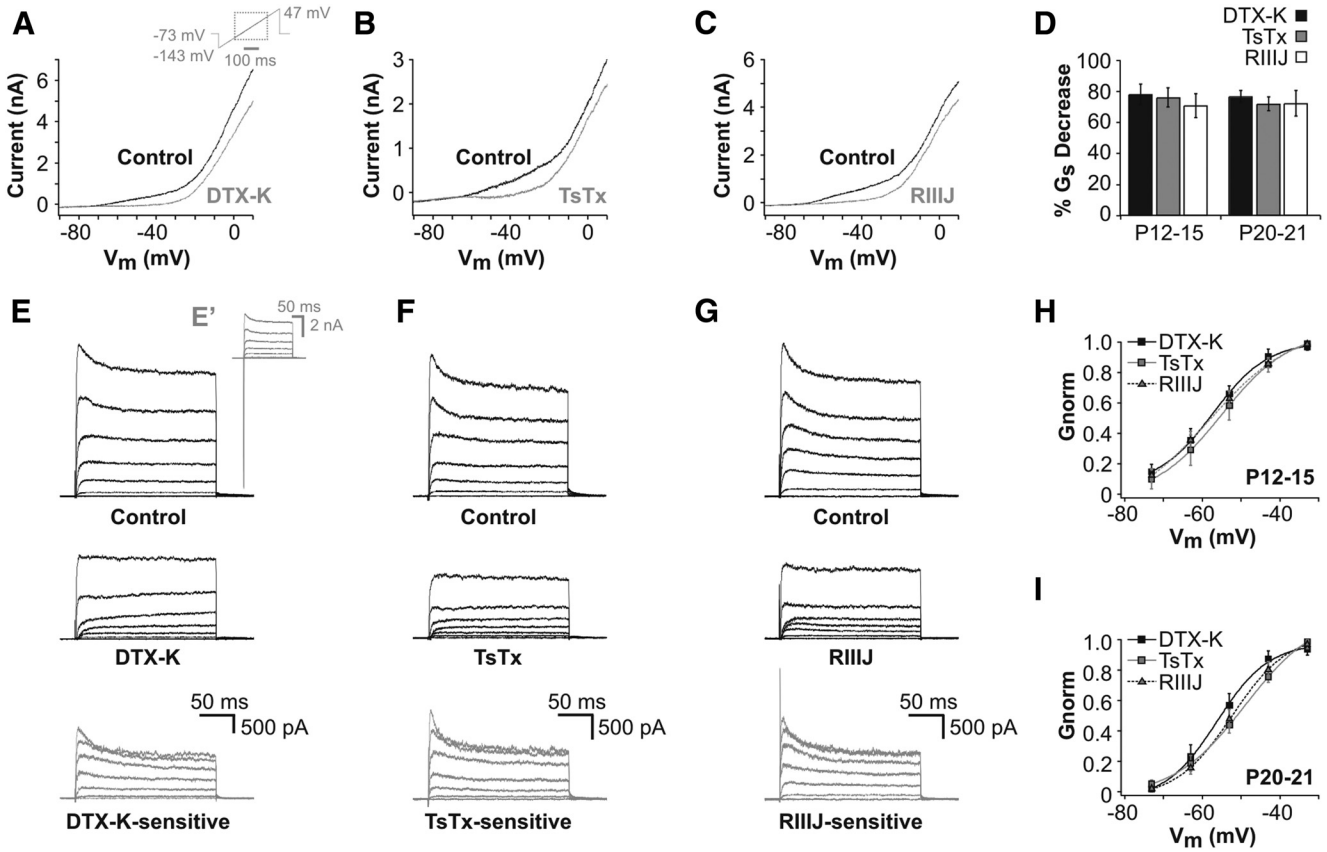

Figure 2. Low-threshold voltage-activated currents in cultured SGNs are inhibited by Kv1-specific toxins. ***A–C***, Representative current responses to a voltage ramp (***A***, inset) before (Control) and after 100 nM bath applications of DTX-K (***A***), TsTx (***B***), or RIIIJ (***C***). There was a decrease of current following application of all three toxins, most prominently between −70 mV and −20 mV. ***D***, Mean decrease in slope conductance (G_S; measured between −63 mV and −53 mV) following toxin application, indicated for the two age groups. DTX-K: $n = 6$ (P12-P15), $n = 7$ (P20-P21); TsTx: $n = 6$ (P12-P15), $n = 6$ (P20-P21); RIIIJ: $n = 5$ (P12-P15), $n = 7$ (P20-P21). ***E–G***, Representative outward current responses during 200 ms voltage steps in 10 mV increments from a holding potential of −73 mV, before (top) and after (middle) 100 nM bath applications of DTX-K (***E***), TsTx (***F***), or RIIIJ (***G***). Bottom, Subtracted toxin-sensitive currents. For clarity, current traces in ***E–G*** have been cropped to remove large transient inward Na^+ currents (shown in ***E′***, inset) to highlight changes to the outward currents. ***H***, Normalized conductance-voltage plots for DTX-K-sensitive ($n = 6$), TsTx-sensitive ($n = 5$), and RIIIJ-sensitive ($n = 5$) currents in P12-P15 SGNs. ***I***, Normalized conductance-voltage plots for DTX-K-sensitive ($n = 6$), TsTx-sensitive ($n = 6$), and RIIIJ-sensitive ($n = 8$) currents in P20-P21 SGNs. Conductance was calculated from the steady-state toxin-sensitive currents measured at the end of the 200 ms voltage steps described for ***E–G*** and was fitted with a Boltzmann function. Mean Boltzmann parameters are given in Table 1.

Rapid adaptation observed in prehearing SGNs (P3-P8) has been shown to be regulated by an α-dendrotoxin (α-DTX) sensitive conductance, implicating the involvement of the Kv1 family of voltage-gated K^+ (Kv) channels (Mo et al., 2002). Further, current inhibition by DTX-K identified Kv1.1 subunits as key contributors to this adaptive behavior (Mo et al., 2002). Here, the involvement of Kv1.1 subunits in the control of adaptation rate in posthearing SGNs was assessed by the application of 100 nM DTX-K to cells under current clamp (Fig. 1*B*,*C*). Typically, the application of DTX-K enhanced the excitability of SGNs - the number of APs elicited by depolarizing current injection steps was increased and the amplitude of the stimulus current required to evoke an AP was reduced (Fig. 1*B*). The number of APs in response to a 100 pA current step was increased in 8 of 9 cells in the presence of DTX-K (Fig. 1*C*) with one of these cells firing spontaneously as a result of DTX-K application. This enhancement of excitability by DTX-K confirmed that Kv1.1 subunits continue to contribute to the maintenance of rapid adaptation in SGNs from hearing animals.

Kv1.1 subunits can homotetramerize, or they can heteromerically tetramerize with other Kv1 family members to form channels which mediate LVA currents. In auditory neurons, these LVA currents act to reduce membrane resistance, to raise the threshold for AP firing, and to prevent repetitive firing (Brew and Forsythe, 1995; Bal and Oertel, 2001). To examine the potential involvement of heteromeric channels containing Kv1.2, we used a recognized blocker of Kv1.2-containing channels, TsTx (Werkman et al., 1993; Brew et al., 2007) and the more recently described RIIIJ (Chen et al., 2010). Under voltage clamp, a ramp protocol enabled LVA currents to be distinguished from high-threshold voltage-activated (HVA) currents in P12-P15 and P20-P21 SGNs (Fig. 2*A*–*C*). The application of 100 nM DTX-K caused a substantial reduction in the LVA current amplitude (Fig. 2*A*), confirming the presence of Kv1.1 subunits. In separate experiments, the application of 100 nM TsTx (Fig. 2*B*) or 100 nM RIIIJ (Fig. 2*C*) produced a comparable reduction in the LVA current amplitude, suggesting a coinvolvement of Kv1.2 subunits. To compare the efficacies of the Kv1.1- and Kv1.2-specific toxins in blocking the LVA current, the change in slope conductance between −63 and −53 mV was calculated (Fig. 2*D*). Reductions in the slope conductance in the presence of DTX-K, TsTx, or RIIIJ were comparable, with no significant differences between the two age groups (toxin comparisons: $p = 0.52$, age comparisons: $p = 0.94$, two-way ANOVA).

To examine the toxin-sensitive currents in more detail, a voltage step protocol was used, with currents being elicited by

Table 1. Boltzmann parameters for toxin-sensitive SGN conductances

	P12-P15			P20-P21		
	$V_{1/2}$ (mV)	*k* (mV)	*n*	$V_{1/2}$ (mV)	*k* (mV)	*n*
DTX-K	−59.4 ± 2.6	7.8 ± 1.4	6	−54.8 ± 2.2	6.1 ± 0.5	6
TsTx	−56.5 ± 3.9	8.6 ± 0.4	5	−50.4 ± 2.0	9.2 ± 0.8	6
RIIIJ	−58.5 ± 2.5	10.4 ± 1.3	5	−52.2 ± 1.8	6.6 ± 0.2	8

Voltage of half-maximal activation ($V_{1/2}$) and slope (*k*) values for the three toxin-sensitive conductances at the two different age groups. Data are mean ± SE; *n* indicates the number of cells.

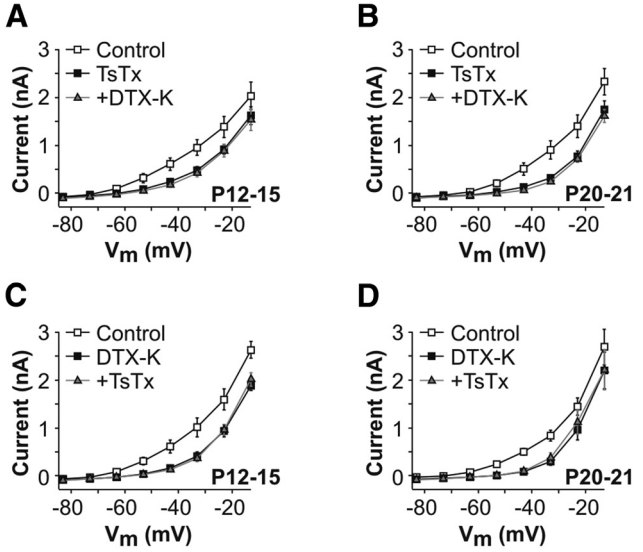

Figure 3. Low-threshold voltage-activated currents in SGNs are mediated via heteromeric channels containing Kv1.1 and Kv1.2 subunits. ***A***, ***B***, Mean steady-state current–voltage relationships before (Control), following TsTx application (100 nM), and following TsTx with DTX-K coapplied (both 100 nM) to SGNs in P12-P15 (***A***; $n = 5$) and P20-P21 (***B***; $n = 6$) cultures. After the initial block by TsTx, there was no additive effect observed upon the addition of DTX-K to the bath. ***C***, ***D***, There was also a lack of additive effect when the toxins were applied in the reverse order to SGNs in P12-P15 (***C***; $n = 6$) and P20-P21 (***D***; $n = 5$) cultures.

200 ms depolarizing steps in 10 mV increments from a holding potential of −73 mV (Fig. 2*E–G*). Following application of the toxins, HVA currents remained that were fast-activating and noninactivating (Fig. 2*E–G*, middle panels). Subtraction of the currents in the presence of the toxins from the control currents revealed the toxin-sensitive currents (Fig. 2*E–G*, bottom). To examine the voltage dependence, conductances were calculated from the steady-state toxin-sensitive currents and plotted against membrane potential for the two different age groups (Fig. 2*H*,*I*). Half-maximal activation ($V_{1/2}$) and slope (*k*) values were calculated by fitting Boltzmann functions to the data (Table 1). Although there was no significant difference in either $V_{1/2}$ or *k* values for the effect of the toxins, there was a small but significant effect in the $V_{1/2}$ and *k* values as a function of age ($V_{1/2}$, toxin comparisons: $p = 0.36$, age comparisons: $p = 0.0084$, two-way ANOVA; *k*, toxin comparisons: $p = 0.059$, age comparisons: $p = 0.021$, two-way ANOVA).

The comparable extent of block (Fig. 2*D*) and voltage dependence (Fig. 2*H*,*I*) of the three toxin-sensitive currents implied that the LVA channels were heteromers containing both Kv1.1 and Kv1.2 subunits. Alternatively, there could be subpopulations of Kv1.1 homomeric and Kv1.2 homomeric channels in SGNs. To address this possibility, TsTx and DTX-K were added sequentially to the bath, to examine whether the second toxin resulted in an additional block (Fig. 3). After the prior application of 100 nM TsTx, coapplication of 100 nM DTX-K did not enhance the inhibition of the LVA current in either age group (Fig. 3*A*,*B*). Application of the toxins in the reverse order also showed no additive effect (Fig. 3*C*,*D*), suggesting that heteromeric Kv1.1/Kv1.2 channels likely mediate the LVA current in cultured SGNs. In a manner comparable to the effect of DTX-K on SGN adaptation (Fig. 1*C*), in the majority of recordings TsTx (4 of 5 cells, P12-P15) and RIIIJ (2 of 3 cells, P12-P15; 5 of 7 cells, P20-P21) slowed adaptation (data not shown).

Kv1.1 and Kv1.2 subunits localize to key neuronal loci

The targeting of ion channel subtypes to particular neuronal loci is highly regulated to ensure the efficient generation and subsequent propagation of APs (Jensen et al., 2011). Following the pharmacological identification of functional Kv1.1 and Kv1.2 subunits in our dissociated SGN cultures, we sought to define more clearly the subcellular localization of these subunits within SGNs in the cochlea. To this end, immunofluorescence experiments on fixed cochlear sections from P20 animals were performed. The somata of SGNs reside in the spiral ganglion with their peripheral neurites extending from the sensory IHCs and their central neurites projecting toward the brainstem (detected using an anti-β3-tubulin antibody; Fig. 4*A*). As suggested by our preceding electrophysiological recordings from dissociated SGNs, immunofluorescence for Kv1.1 and Kv1.2 subunits was localized to SGN somata, with prominent membrane expression (Fig. 4*B*). This membrane expression was continuous as the somata tapered into the proximal portion of peripheral and central neurites but then ended abruptly at positions corresponding to juxtaparanodal structures (Fig. 4*C*).

Although not thought to be a prominent component of all nodes of Ranvier in the PNS (Devaux et al., 2003), immunofluorescence for HVA current-mediating Kv3.1b subunits localized to discrete puncta at the perisomatic nodes of all SGNs (Fig. 4*C*, arrowheads) but was largely absent from the somatic membrane. A comparable discrete perisomatic pattern of expression has been reported previously for voltage-gated sodium (Nav) channels and indicates that APs must propagate across the soma despite an apparent lack of somatic Nav channels (Hossain et al., 2005). In addition to the highly organized expression within the somatic membrane, Kv1.2 immunofluorescence was observed within juxtaparanodes throughout both the peripheral and central neurites (Fig. 5*A*). Kv1.1 colocalized with Kv1.2 at all these juxtaparanodal clusters (Fig. 5*B*), further suggesting these subunits could combine to form functional heteromers. Consistent with the nodal arrangement observed within the proximal peripheral and central neurites (Fig. 4*C*), immunofluorescence for both Nav and Kv3.1b subunits was detected at the center of the flanking Kv1.1/Kv1.2 clusters in both central (Fig. 5*C*,*D*) and peripheral neurites (Fig. 5*E*,*F*).

Kv1.2 immunofluorescence was also observed in a region underneath the IHC synaptic region (Figs. 5*A*, 6*A–D*). The peripheral neurites of SGNs extend from the ganglion and are housed within the osseous spiral lamina until they reach the cochlear periphery. The peripheral neurites are almost continually myelinated along the length of the spiral lamina (Nayagam et al., 2011), but myelination ceases just before the habenula perforata (Fig. 6*A*), where they enter the organ of Corti. Kv1.1 and Kv1.2 subunits colocalized to the peripheral neurites at the region where myelination terminates (Fig. 6*B*). Nav channels have been shown to localize to the subsequent unmyelinated segment of the neurites close to the habenula perforata, forming the site of spike generation for SGNs (Hossain et al., 2005). Here, we found that

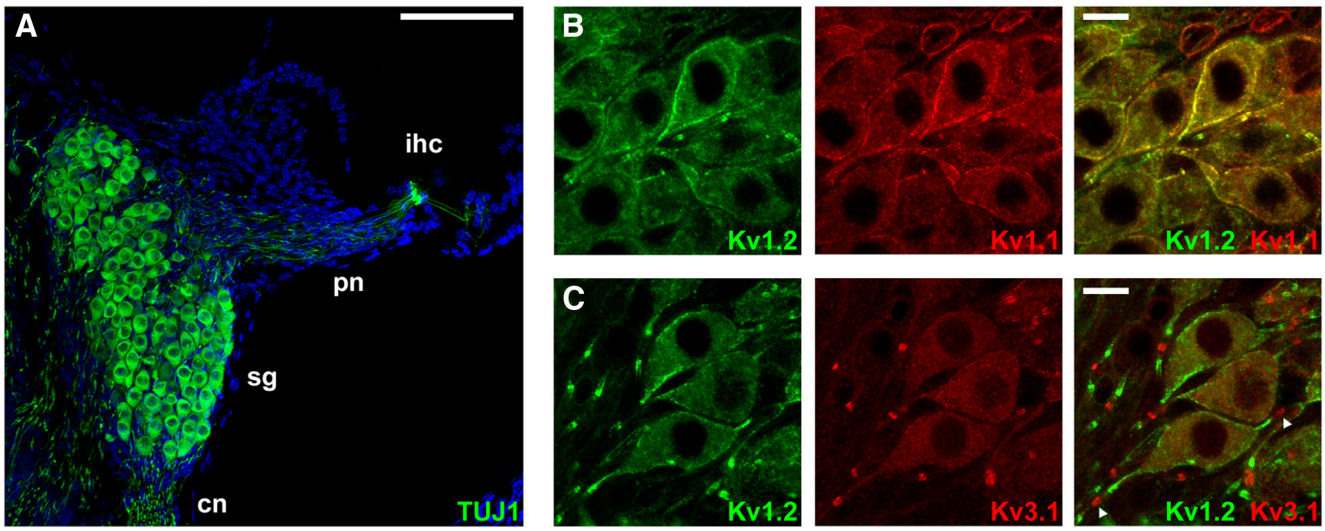

Figure 4. Kv1.1 and Kv1.2 subunits localize to SGN somata. ***A***, TUJ1 labels SGNs in a mouse P20 cochlear section. SGN somata reside within the spiral ganglion (sg) with peripheral neurites (pn) extending toward the inner hair cell (ihc) and central neurites (cn) projecting to the brainstem. Scale bar, 100 μm (20 μm *z*-projection). ***B***, Kv1.2 and Kv1.1 immunofluorescence is detected in SGN somata with prominent membrane expression. Kv1.1 is also detected in glial cells (2 cells can be observed top middle and top right of middle panel). ***C***, Presomatic and postsomatic nodes of Ranvier contain Kv3.1b subunits (arrowheads). Kv1.2 immunofluorescence flanks these nodes. ***B***, ***C***, Right panels, Overlay of the two channels displayed in the left and center panels. Scale bars: ***B***, ***C***, 10 μm.

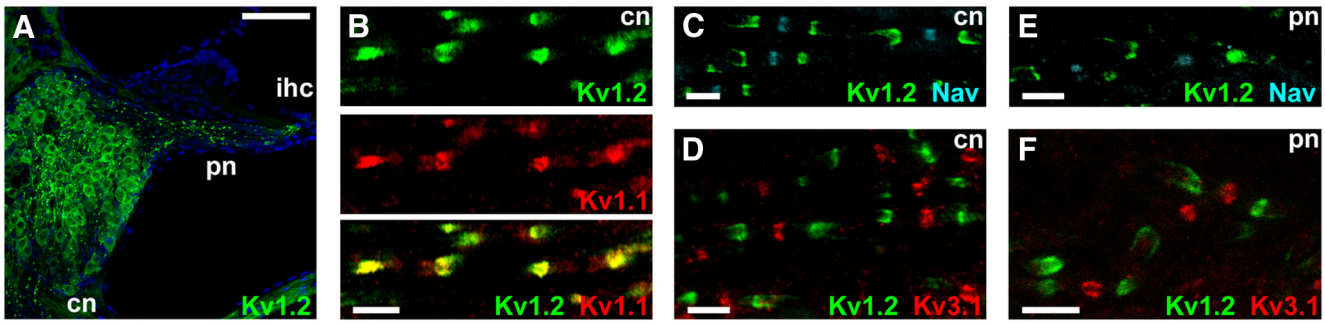

Figure 5. Kv1.1 and Kv1.2 subunits localize to juxtaparanodes in central and peripheral neurites. ***A***, Overview of Kv1.2 immunofluorescence in a mouse P20 cochlear section. In addition to expression in SGN somata, distinct Kv1.2 puncta are observed in both peripheral (pn) and central neurites (cn). Further expression can be seen beneath the inner hair cell (ihc). Scale bar, 100 μm. ***B***, Colocalization of Kv1.1 and Kv1.2 subunits at juxtaparanodes in cn. Bottom, Overlay of the two channels displayed in the top and middle panels. ***C***, ***D***, Nav channels (***C***) and Kv3.1b subunits (***D***) localize to nodes of Ranvier flanked by juxtaparanodal Kv1.2 clusters in cn. ***E***, ***F***, Nav channels (***E***) and Kv3.1b subunits (***F***) are also observed at nodes in pn with juxtaparanodal Kv1.2 immunofluorescence. Scale bars: ***B–F***, 5 μm.

Kv1.2 immunofluorescence was spatially distinct from the Nav channel immunofluorescence, consistent with a "heminodal" arrangement of the two channel types (Fig. 6*C*). The Kv1.1/Kv1.2 coimmunofluorescence is also reminiscent of the 'juxtaparaheminodal' microdomain described in vestibular afferents (Lysakowski et al., 2011). In the cochlea, each unmyelinated neurite ending forms a single synapse with the base of an IHC, which could be marked postsynaptically by anti-PSD95 antibodies (Fig. 6*D*). Because Kv3.1b was identified in the peripheral and central nodes of SGNs (Fig. 5*D*,*F*), its localization at the first heminode was investigated. Kv3.1b was expressed in a similar region to the Nav channels, but notably distinct from the Kv1.2 subunits (Fig. 6*D*). This highly organized distribution of Kv1.1- and Kv1.2-containing channels to key neuronal structures points toward a significant role in the regulation of AP generation and subsequent propagation within the auditory nerve.

Decreasing PIP_2 production enhances excitability of posthearing SGNs

The contribution of Kv1.1/Kv1.2 heteromeric channels to the LVA current in cultured SGNs, and their specific targeting to key neuronal loci *in vivo*, points to important roles for this channel in the dynamic regulation of excitability of the auditory nerve. Consequently, we next sought to identify endogenous modulators of the channels, which might be manipulated to provide external control of neuronal firing properties. PIP_2 is a recognized regulator of ion channel activity and has been shown to modulate a number of K^+ channels (Suh and Hille, 2008). Recently, in a heterologous expression system, depletion of PIP_2 has been shown to specifically decrease Kv1.2-mediated current amplitudes while also adjusting the voltage dependence of the channels (Rodriguez-Menchaca et al., 2012; Kruse and Hille, 2013). This effect on Kv1.2-containing channels led us to examine the effect of PIP_2 on SGN excitability. To this end, basal turn P12-P15 cultures were pretreated with the phosphoinositide (PI) kinase inhibitor wortmannin (Fig. 7*A*). At low concentrations (~100 nM), wortmannin inhibits PI3-kinase (PI3K), resulting in reduced production of PIP_3 (Yano et al., 1993). At higher concentrations (~10 μM), wortmannin also inhibits PI4-kinase (PI4K), resulting in a reduced production of cellular PIP_2 (Fruman et al., 1998). SGNs were pooled in terms of the number of APs evoked in response to a 200 ms depolarizing current injection (100 pA):

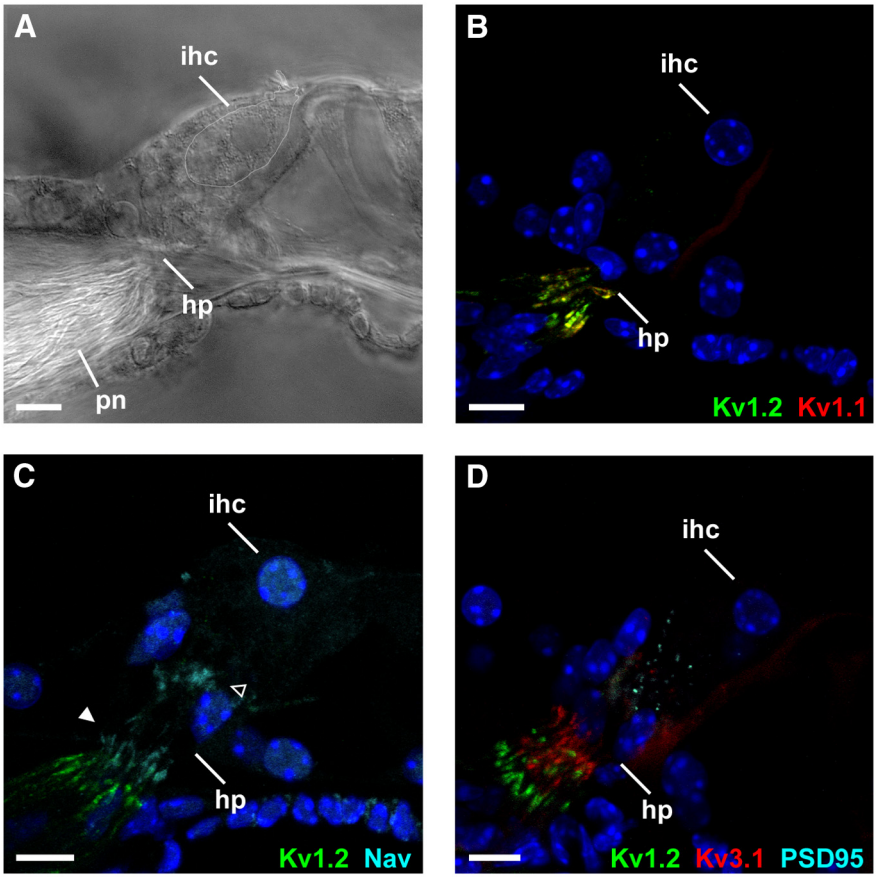

Figure 6. Kv1.1 and Kv1.2 subunits are localized to the first heminode in SGNs. ***A***, DIC image showing the organization of the inner hair cell (ihc) region of the organ of Corti. Peripheral neurites (pn) are myelinated until their approach into the Organ of Corti via the habenula perforata (hp) where they form a single synapse with an ihc. ***B***, Kv1.2 and Kv1.1 subunits localize to the pn of SGNs in the region where myelination ceases. ***C***, Nav channels are located to discrete regions of the pn, where they form the initial spike generator of SGNs (filled arrowhead). No overlap is observed with Kv1.2 immunofluorescence. Nav channels also localize beneath the IHCs (open arrowhead), but 3D projections reveal that these immunofluorescent fibers run parallel to the IHC rows and most likely correspond to efferent neurites (Warr and Boche, 2003). ***D***, Kv3.1b subunits are localized to the same region as Nav channels, with Kv1.2 subunits more distally located to the synapses marked by PSD-95. Scale bars: ***A–D***, 10 μm.

rapidly adapting, 0–1 APs; slowly adapting, 2–9 APs; nonadapting, ≥10 APs. In SGNs preincubated with vehicle only (Control), 9 of 12 adapted rapidly, with the remaining cells adapting slowly. Preincubation of SGN cultures with 100 nM wortmannin had no effect on this pooling of firing phenotypes, suggesting that PIP_3 availability did not influence SGN excitability. However, preincubation with 10 μM wortmannin resulted in a reduced proportion of rapidly adapting neurons (7 of 18), and an increased proportion of nonadapting neurons (6 of 18), with the remaining neurons slowly adapting (5 of 18). This suggested that PIP_2 depletion, via PI4K inhibition, could enhance excitability within the SGN population. In separate experiments, the nonhydrolysable PIP_2 analog diC_8PIP_2 was applied intracellularly during recordings from SGNs preincubated with 10 μM wortmannin. Under these conditions, the effects of wortmannin on excitability were negated, with the proportion of rapidly adapting cells being identical to control conditions (75%; 6 of 8), suggesting that the effect of wortmannin on rapidly adapting neurons was associated with PIP_2 depletion.

PIP_2 sequestration slows adaptation in SGNs via inhibition of the LVA current

To further examine the effects of PIP_2 modulation on SGN excitability, we used a membrane-targeting palmitoylated peptide with a high binding affinity for PIP_2 (Robbins et al., 2006). The PIP_2-PP consists of a 10 amino acid chain identical to the putative PIP_2 binding sequence of Kv7.2–7.5 subunits, and palmitoylation ensures it specifically targets the plasma membrane to sequester PIP_2. Bath application of 3 μM PIP_2-PP to rapidly adapting SGNs (P12-P15) enhanced their excitability (Fig. 7*B–D*). The extent of this enhancement was variable, with some SGNs becoming more slowly adapting (Fig. 7*B*,*D*) whereas others became nonadapting (Fig. 7*C*,*D*). In addition to increasing the number of APs, PIP_2-PP significantly augmented the steady-state voltage during the current injection step ($n = 4$, $p < 0.001$, two-way ANOVA; Fig. 7*E*), indicating an increased membrane resistance.

The increased membrane resistance pointed to a decreased activity of Kv channels following PIP_2 sequestration. Accordingly, separate voltage-clamp recordings revealed an underlying inhibition of an LVA current (Fig. 8*A*,*B*). Comparison of the current–voltage relationship of the PIP_2-PP-sensitive and DTX-K-sensitive currents from age-matched (P12-P15) SGN cultures revealed almost identical plots (Fig. 8*C*). Inclusion of diC_8PIP_2 in the recording pipette decreased the extent and slowed the rate of PIP_2-PP-dependent inhibition of the LVA current (Fig. 8*D*,*E*), suggesting that the effects of PIP_2-PP were indeed mediated via PIP_2 depletion and not via a direct block of the underlying channels. In an attempt to target endogenous phosphoinositide signaling pathways, two alternative approaches were used to diminish PIP_2 levels. The application of oxotremorine-M (10 μM), a broad agonist of Gq-coupled muscarinic receptors (Birdsall et al., 1978), resulted in a small but nonsignificant inhibition of the LVA current (8.1 ± 2.6% inhibition at −53 mV, $n = 5$, $p = 0.054$, paired Student's *t* test). m-3M3FBS (10 μM), a phospholipase-C activator (Bae et al., 2003), had variable effects between cells, with some showing a decrease and others an increase in LVA current (11.8 ± 8.2% inhibition at −53 mV, $n = 8$, $p = 0.93$, paired Student's *t* test).

To confirm whether PIP_2-PP was inhibiting Kv1 channels, toxin coapplication experiments were performed (Fig. 8*F*,*G*). Following prior application of 3 μM PIP_2-PP, the addition of 100 nM DTX-K to the bath failed to further reduce the LVA current amplitude (Fig. 8*F*). Reversing the order of the PIP_2-PP and DTX-K applications also failed to enhance the inhibition (Fig. 8*G*), suggesting that PIP_2-PP and DTX-K were targeting the same channels. This finding indicates that the Kv1.1/Kv1.2 channels regulating excitability of SGNs can be modulated by cellular PIP_2.

PIP_2 sequestration inhibits currents mediated by Kv1.1/Kv1.2 heteromeric channels

Previous examination of Kv1.1, Kv1.3, Kv1.4, and Kv1.5 homomeric channels expressed in heterologous systems has revealed an apparent lack of influence of PIP_2 on these members of the Kv1 subfamily (Kruse et al., 2012). Kv1.2 homomeric channels, how-

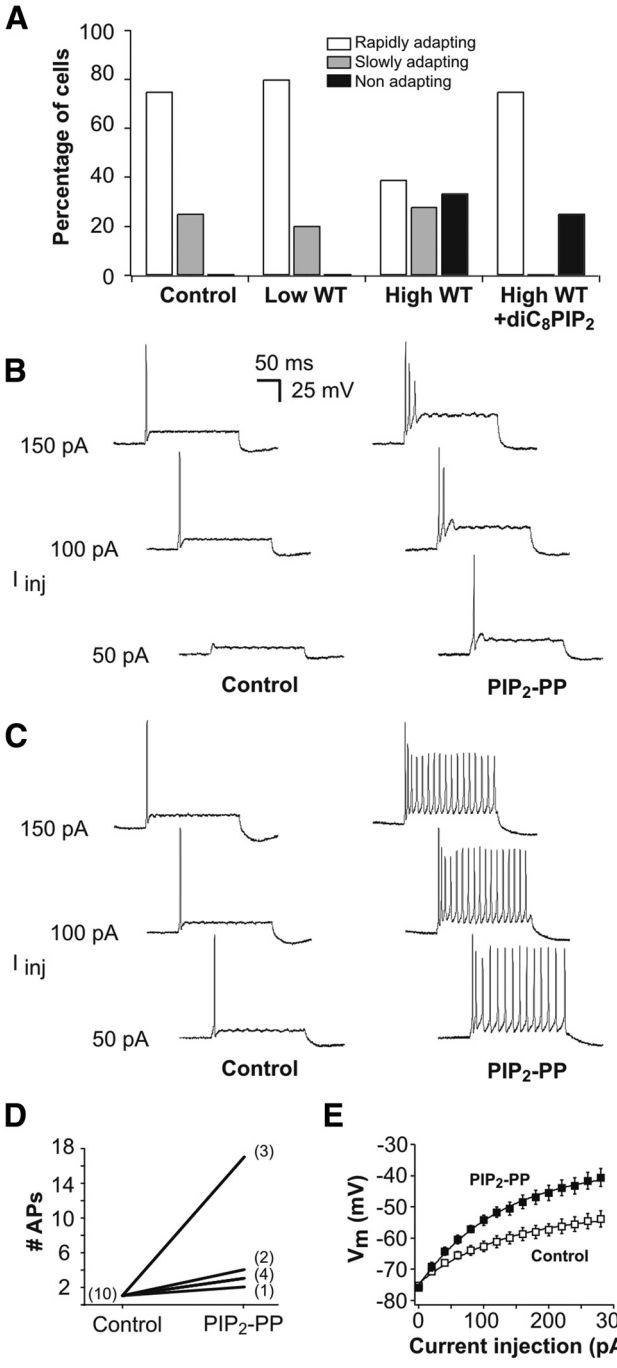

Figure 7. PIP_2 depletion enhances the excitability of posthearing SGNs. ***A***, The distribution of AP firing phenotypes within the population of cultured SGNs depended on the availability of cellular PIP_2. SGNs preincubated for 1 h in 0.1% DMSO (Control, $n = 12$) were predominantly rapidly adapting, as were SGNs preincubated in 100 nM wortmannin ("Low WT," $n = 10$). SGNs preincubated in 10 μM wortmannin ("High WT," $n = 18$) displayed a more heterogeneous firing behavior, with a reduced proportion of rapidly adapting cells. When diC_8PIP_2 (100 μM) was applied intracellularly during recordings from SGNs preincubated in 10 μM wortmannin ("High WT + diC_8PIP_2," $n = 8$), the proportion of rapidly adapting cells returned to control levels. ***B***, ***C***, Representative voltage responses from two SGNs to depolarizing current injections, before (Control, left) and after the bath application of 3 μM PIP_2-PP (right). Typically, PIP_2-PP slowed the rate of adaptation and reduced the current required to elicit AP firing. The 200 ms current injections were applied in 50 pA increments from a holding potential of −73 mV. ***D***, Summary of the effect of 3 μM PIP_2-PP on the number of APs (#APs) elicited in response to a 100 pA current step (number of cells is shown in parentheses). ***E***, Comparison of the mean voltage–current relationship before (Control) and after the bath application of 3 μM PIP_2-PP ($n = 4$). Steady-state voltage was measured 10 ms from the end of 600 ms current injections applied in 20 pA increments from a holding potential of −73 mV.

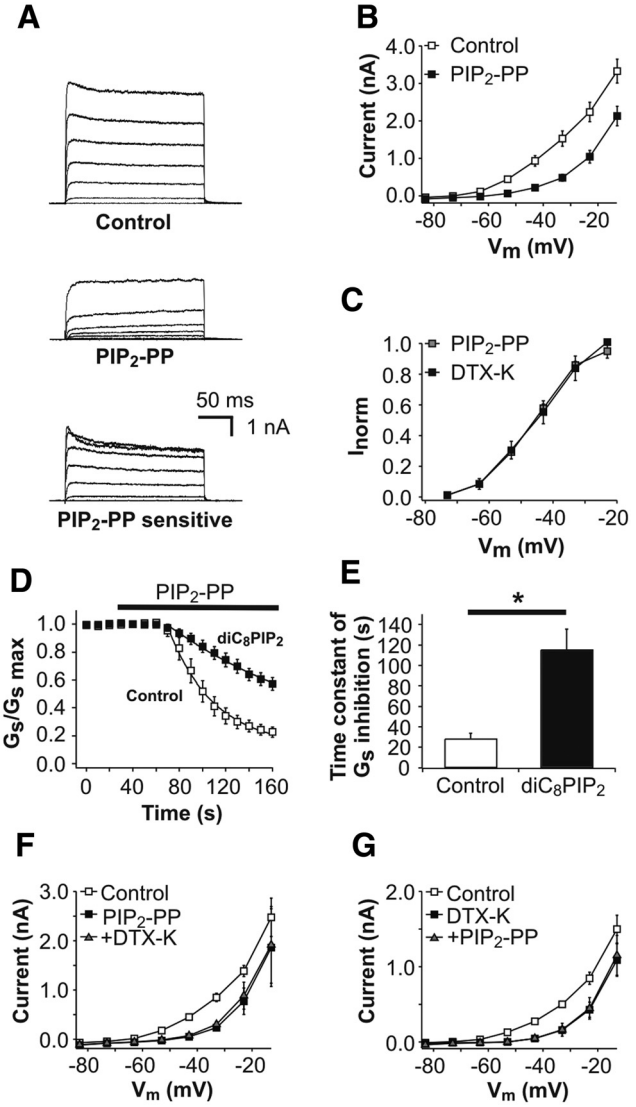

Figure 8. PIP_2 sequestration inhibits the Kv1-mediated low-threshold voltage-activated current in SGNs. ***A***, Representative outward current responses during 200 ms voltage steps in 10 mV increments from a holding potential of −73 mV, before (Control, top) and after (middle panel) bath application of PIP_2-PP (3 μM). Bottom, Subtracted PIP_2-PP-sensitive currents. ***B***, Mean steady-state current–voltage relationships before (Control) and after PIP_2-PP application (3 μM; $n = 13$). Steady-state currents were measured at the end of the voltage steps described for ***A***. ***C***, Comparison of normalized steady-state current–voltage plots of the PIP_2-PP-sensitive (PIP_2-PP; 3 μM; $n = 13$) and DTX-K-sensitive currents (DTX-K; 100 nM; $n = 6$). ***D***, Normalized slope conductance (G_s), calculated from a voltage ramp protocol applied every 10 s (as described for Fig. 2*A–D*), decreased during the bath application of PIP_2-PP (Control; 1 μM; $n = 5$). Inclusion of diC_8PIP_2 (200 μM) in the intracellular solution reduced the effect of PIP_2-PP (diC_8PIP_2; $n = 7$). ***E***, Comparison of the rates of G_s inhibition induced by PIP_2-PP in the absence (Control; $n = 5$) and presence of diC_8PIP_2 (200 μM) in the intracellular solution (diC_8PIP_2; $n = 7$). The time constant of G_s inhibition was calculated by fitting monoexponential functions to the data in ***D***. $^*p < 0.05$. ***F***, Mean current–voltage relationships of SGNs before (Control), following the application of PIP_2-PP (3 μM), and following subsequent coapplication of PIP_2-PP with DTX-K (+DTX-K; 100 nM; $n = 3$). After the initial block by PIP_2-PP, there was no additive effect observed upon the addition of DTX-K to the bath. ***G***, There was also a lack of additive effect when the drugs were applied in the reverse order ($n = 3$).

ever, are regulated by PIP_2 binding, with an ~20% reduction in current amplitude and a negative shift in the $V_{1/2}$ of activation upon PIP_2 depletion (Rodriguez-Menchaca et al., 2012; Kruse and Hille, 2013). The results of molecular dynamics simulations suggest that this change in voltage dependence may result from

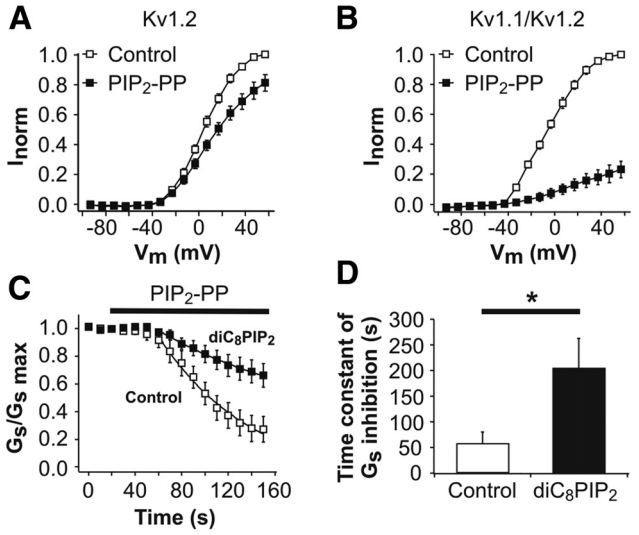

Figure 9. PIP_2 sequestration preferentially inhibits Kv1.2 heteromeric channels expressed in HEK293 cells. ***A***, Normalized steady-state current–voltage plots for Kv1.2 homomeric channels before (Control) and after the application of PIP_2-PP (PIP_2-PP; 1 μM; $n = 6$). ***B***, Normalized steady-state current–voltage plots for Kv1.1/Kv1.2 channels before (Control) and after the application of PIP_2-PP (1 μM; $n = 5$). ***A***, ***B***, Steady-state currents were measured at the end of 200 ms voltage steps applied in 10 mV increments from a holding potential of −73 mV. There was no significant difference in the control current amplitudes of Kv1.2 and Kv1.1/Kv1.2 (mean current density, Kv1.2: 599 ± 227 pA/pF; Kv1.1/Kv1.2, 624 ± 258 pA/pF; $p = 0.85$, unpaired Student's *t* test). ***C***, Normalized slope conductance (G_s) of Kv1.1/Kv1.2, calculated from a voltage ramp protocol applied every 10 s (as described for Fig. 2*A–D*), decreased during application of PIP_2-PP (Control; 1 μM; $n = 7$). The addition of diC_8PIP_2 (200 μM) to the intracellular solution reduced the effect of PIP_2-PP (diC_8PIP_2; $n = 5$). ***D***, Comparison of the rate of Kv1.1/Kv1.2 G_s inhibition by PIP_2-PP in the absence (Control; $n = 7$) and presence of diC_8PIP_2 (200 μM) in the intracellular solution (diC_8PIP_2; $n = 5$). The time constant of G_s inhibition was calculated by fitting monoexponential functions to the G_s data in ***C***. *$p < 0.05$.

the influence of PIP_2 binding on voltage-sensor movement (Abderemane-Ali et al., 2012). The magnitude of the hyperpolarizing shift varied between ~14 mV in *Xenopus* oocytes (Rodriguez-Menchaca et al., 2012) and ~3 mV in a human embryonic kidney cell line (Kruse and Hille, 2013). To investigate the effects of PIP_2-PP application on Kv1.2 homomeric channels, we expressed Kv1.2 in HEK293 cells. Consistent with the findings of others, we observed a reduction of Kv1.2 current amplitude after the application of PIP_2-PP (18.6 ± 5.5% at 57 mV, $n = 6$; Fig. 9*A*). However, no significant change in the $V_{1/2}$ of activation was observed after the application of PIP_2-PP (Control: $V_{1/2} = -11.7 \pm 2.2$ mV; PIP_2-PP: $V_{1/2} = -11.3 \pm 2.2$ mV, $n = 6$, $p = 0.64$, paired Student's *t* test).

The considerably greater reduction of the LVA current in SGNs by PIP_2-PP application and our proposal that Kv1.1/Kv1.2 heteromeric channels likely mediate this current, led us to investigate the effects of PIP_2-PP application on Kv1.1/Kv1.2 heteromeric channels. The application of PIP_2-PP to Kv1.1/Kv1.2 currents resulted in a more substantial reduction in amplitude (77.7 ± 5.1% at 57 mV, $n = 5$; Fig. 9*B*) compared with its effect on homomeric Kv1.2 channels ($p = 0.00003$, unpaired Student's *t* test). Again, there was no significant shift in the $V_{1/2}$ of activation (Control: $V_{1/2} = -21 \pm 3.7$ mV; PIP_2-PP: $V_{1/2} = -19.7 \pm 6$ mV, $n = 4$, $p = 0.63$, paired Student's *t* test). Intracellular dialysis with diC_8PIP_2 produced a marked decrease, and slowing of the rate, of inhibition by PIP_2-PP (Fig. 9*C*,*D*) suggesting that the effect of PIP_2-PP on Kv1.1/Kv1.2 channels was indeed caused by PIP_2 sequestration. The increased sensitivity of Kv1.1/Kv1.2 to PIP_2-PP may reflect a lower affinity of the heteromeric channels for PIP_2 compared with Kv1.2 homomers, allowing PIP_2-PP to compete more effectively for channel-bound PIP_2. A similar reasoning has been used to explain the surprising ineffectiveness of PIP_2-PP in sequestering PIP_2 from the highly PIP_2-dependent Kir2.1 channel (Robbins et al., 2006). Notably, the reduction of heterologous Kv1.1/Kv1.2 currents by PIP_2-PP resembled its effect on the LVA current in SGNs, providing further support for the proposal that the LVA current is mediated by Kv1.1/Kv1.2 heteromers.

Discussion

The LVA current is necessary for rapid adaptation in auditory neurons

Kv1.1 and Kv1.2 subunits appear targeted to specific functional loci within afferent neurons of the auditory nerve, in a manner that points to key roles in spike generation and propagation. This improved description of Kv1 channel localization, and how LVA K^+ currents may contribute, is essential for more accurate models of auditory nerve function in the normal and hearing-impaired cochlea. LVA currents control adaptation throughout the auditory pathway, as described in neurons of the ventral cochlear nucleus (Manis and Marx, 1991; Schwarz and Puil, 1997), the medial nucleus of the trapezoid body (MNTB) (Brew and Forsythe, 1995), and the medial (Smith, 1995) and lateral (Barnes-Davies et al., 2004) superior olives. As described here and previously for SGNs (Mo et al., 2002) and other auditory neurons (Brew and Forsythe, 1995; Smith, 1995; Schwarz and Puil, 1997; Bal and Oertel, 2001), LVA current inhibition results in slowed adaptation. Within the auditory pathway, EPSCs are often severalfold larger than the threshold required to elicit postsynaptic APs (Johnston et al., 2009; Grant et al., 2010; Rutherford et al., 2012), minimizing timing delays and ensuring fast AP transmission. Rapid adaptation ensures that auditory neurons fire phasically in response to these large depolarizing stimuli, thus maintaining temporal fidelity and phase synchronization (Johnston et al., 2010).

Recordings from cultured SGNs reveal a variety of adaptive firing behaviors (Adamson et al., 2002; Lv et al., 2012; Crozier and Davis, 2014). An association between firing rate and tonotopic location was proposed for SGNs in prehearing mice (P3-P8), where all SGNs originating from the basal turn were rapidly adapting while apical SGNs displayed rapid or slower adaptation (Adamson et al., 2002). The rapidly adapting phenotype was associated with Kv1-mediated currents, which were larger in basally derived SGNs (Liu et al., 2014). Conversely, studies from posthearing mice have described more heterogeneous firing properties (Lv et al., 2012; current study). It is not certain, though, that the firing properties of cultured SGNs accurately represent their behavior *in vivo*. In afferent bouton recordings from isolated cochlear preparations, all SGNs fire single APs in response to sustained depolarizing stimuli, suggesting that rapid adaptation may be a consistent feature of functionally mature SGNs (Rutherford et al., 2012). Rapid adaptation is also a dominant feature of somatic recordings from Type I SGNs in rat cochlear slice preparations (Jagger and Housley, 2002, 2003). The apparent ubiquity of the adaptation mechanism suggests that it deserves further study, and our approach using cultured SGNs enabled us to dissect its molecular basis in the functionally mature cochlea.

Kv1.1/Kv1.2 heteromeric channels mediate LVA currents in mature SGNs

The most parsimonious explanation of our pharmacology data is that channels containing both Kv1.1 and Kv1.2 subunits mediate the LVA current in posthearing SGNs. Kv1.1- and Kv1.2-specific toxins displayed comparable levels of current inhibition, and their effects were not additive, and so we propose that these subunits comprise a heteromer, rather than two subpopulations of homomeric channels. Kv1.1/Kv1.2 heteromeric channels have been identified elsewhere within the auditory pathway, including the MNTB where they ensure rapid adaptation (Dodson et al., 2002). The properties of auditory neurons in Kv1.1-null and Kv1.2-null mutants have been assessed, but due to the heteromeric nature of the channels, interpretation of the results can be problematic. The remaining functional subunit(s) may still form channels, or there may be compensatory effects from other Kv subunits (Brew et al., 2003, 2007; Wang et al., 2013). In Kv1.2-null mice, both MNTB neurons (Brew et al., 2007) and SGNs (Wang et al., 2013) displayed larger LVA currents and were hypoexcitable compared with wild-type cells. This phenotype could be explained by the biophysical properties of remaining Kv1.1 subunits, which may form homomeric channels in the absence of Kv1.2. The more hyperpolarized threshold of activation and half-maximal voltage of activation of Kv1.1 channels could account for the increased LVA current amplitude and the resulting hypoexcitability (Brew et al., 2007). Our results do not rule out the presence of other subunits within the Kv1.1/Kv1.2 heteromer. It was recently proposed that Kv1.4 subunits may be present in the channels (Wang et al., 2013). However, we did not observe substantial inactivation of the LVA current that Kv1.4 subunits would convey (Po et al., 1993; Nunoki et al., 1994), nor did we detect Kv1.4 immunofluorescence in cochlear sections (data not shown).

Mutually exclusive localization of Kv1 and Kv3 subunits within neuronal microdomains contributes to regulation of AP initiation and propagation

The specific targeting of Kv1.1 and Kv1.2 subunits to the somatic membrane, to juxtaparanodes, and to the first heminode implicate Kv1.1/Kv1.2-containing channels in the control of AP generation and propagation. APs are initiated in the auditory and vestibular systems at the first heminode of the peripheral neurites (Hossain et al., 2005; Lysakowski et al., 2011). Patch-clamp recordings from SGN boutons have revealed the presence of an LVA K^+ current in this region (Yi et al., 2010). Our immunofluorescence experiments, which localize Kv1.1 and Kv1.2 subunits to the first heminode, identify Kv1.1/Kv1.2 channels as candidate mediators for this LVA current. In addition to their role in determining rapid adaptation, Kv1 channels at AP initiation zones contribute to shortened AP latency and reduced jitter (Johnston et al., 2010). Along with channels mediating I_h (Yi et al., 2010), Kv1 channels open at rest contribute to low input resistance, reducing the membrane time constant and enhancing temporal precision. Furthermore, the activation of Kv1 channels by depolarizing stimuli acts as a high-pass filter, inhibiting AP firing in response to slow EPSCs. Only fast depolarizations, which reach threshold before activating sufficient Kv1 channels to oppose the depolarization, result in APs. Depolarizing rate thresholds have been identified in several auditory neurons, including within the MNTB (Gittelman and Tempel, 2006) and ventral cochlear nucleus (McGinley and Oertel, 2006), as well as in SGNs (Rutherford et al., 2012), and are proposed to be mediated by Kv1 channels. These features establish a temporal window for AP initiation (Gittelman and Tempel, 2006), thus reducing the variability of AP latencies (i.e., jitter).

Kv1.1 and Kv1.2 subunits have been identified at myelinated juxtaparanodes in both CNS (Wang et al., 1993) and PNS axons (Mi et al., 1995; Rasband et al., 1998; Rasband and Trimmer, 2001). Proposed roles for juxtaparanodal Kv1 channels include maintenance of the internodal resting membrane potential and prevention of spike reentry into nodes of Ranvier, although the extent of channel activation under the myelin sheath is somewhat contested (Arancibia-Carcamo and Attwell, 2014). In all neuronal loci here, localization of Kv1 subunits was spatially distinct from that of Kv3.1b subunits, suggesting that there are highly regulated processes determining the location of these subunits within the cell membrane. The apparent targeting of Kv3.1b subunits to all SGN nodes of Ranvier is contrary to observations elsewhere in the PNS (Devaux et al., 2003) and may point to a specialization of the auditory nerve enabling the transmission of high-frequency information.

PIP_2 regulates SGN excitability via Kv1-containing channels

PIP_2 is a major phosphoinositide in the eukaryotic plasma membrane and an important regulator of K^+ channels (Suh and Hille, 2008). In heterologous expression systems, PIP_2 depletion causes a modest reduction (~20%) in current amplitude of Kv1.2 homomeric channels with a concomitant negative shift in the activation curve (Rodriguez-Menchaca et al., 2012; Kruse and Hille, 2013). Utilizing PIP_2-PP, a membrane-targeting peptide to chelate PIP_2 (Robbins et al., 2006), we observed a comparable reduction in current amplitude for Kv1.2 homomeric channels expressed in HEK293 cells. Interestingly, in cells coexpressing Kv1.1 subunits with Kv1.2, the sensitivity to PIP_2 depletion was markedly increased and more closely recapitulated our observations in cultured SGNs. Neuronal Kv7 (KCNQ) channels are also notably regulated by PIP_2 (Suh and Hille, 2002), and small Kv7-like currents have been identified in SGNs (Lv et al., 2010). However, we propose that our observations are not due to inhibition of Kv7 channels because blockade of Kv7 channels by linopirdine (Lv et al., 2010) or XE991 (our data; data not shown) did not affect rapid adaptation.

The influence of PIP_2 availability on LVA current amplitude highlights phosphoinositide signaling as an intrinsic regulator of SGN excitability. This may be of particular interest to the field of cochlear implant technology. Excessive current spread from cochlear implant electrodes results in the stimulation of overlapping populations of SGNs. This restricts the number of perceptual frequency channels for cochlear implant users, resulting in suboptimal speech perception and poor appreciation of music (O'Leary et al., 2009). A current translational research focus is to reduce the "neural gap" by encouraging growth of SGN peripheral neurites toward the stimulating electrode (Pinyon et al., 2014). A complementary approach could be to adjust the excitability of SGNs via pharmacological manipulation of global cellular PIP_2 levels, thus minimizing the necessary input energy and optimizing frequency channel activation. At a more physiological level, regulation of Kv1-mediated LVA currents by membrane phosphoinositides may provide control of ion channels within specific molecular microdomains (e.g., the first heminode, juxtaparanodes), to provide local dynamic control of spike initiation and propagation.

References

Abderemane-Ali F, Es-Salah-Lamoureux Z, Delemotte L, Kasimova MA, Labro AJ, Snyders DJ, Fedida D, Tarek M, Baró I, Loussouarn G (2012) Dual effect of phosphatidylinositol (4,5)-bisphosphate PIP(2) on Shaker K(+) channels. J Biol Chem 287:36158–36167. CrossRef Medline

Adamson CL, Reid MA, Mo ZL, Bowne-English J, Davis RL (2002) Firing features and potassium channel content of murine spiral ganglion neu-

rons vary with cochlear location. J Comp Neurol 447:331–350. CrossRef Medline

Arancibia-Carcamo IL, Attwell D (2014) The node of Ranvier in CNS pathology. Acta Neuropathol 128:161–175. CrossRef Medline

Bae YS, Lee TG, Park JC, Hur JH, Kim Y, Heo K, Kwak JY, Suh PG, Ryu SH (2003) Identification of a compound that directly stimulates phospholipase C activity. Mol Pharmacol 63:1043–1050. CrossRef Medline

Bal R, Oertel D (2001) Potassium currents in octopus cells of the mammalian cochlear nucleus. J Neurophysiol 86:2299–2311. Medline

Barnes-Davies M, Barker MC, Osmani F, Forsythe ID (2004) Kv1 currents mediate a gradient of principal neuron excitability across the tonotopic axis in the rat lateral superior olive. Eur J Neurosci 19:325–333. CrossRef Medline

Birdsall NJ, Burgen AS, Hulme EC (1978) The binding of agonists to brain muscarinic receptors. Mol Pharmacol 14:723–736. Medline

Brew HM, Forsythe ID (1995) Two voltage-dependent K^+ conductances with complementary functions in postsynaptic integration at a central auditory synapse. J Neurosci 15:8011–8022. Medline

Brew HM, Hallows JL, Tempel BL (2003) Hyperexcitability and reduced low threshold potassium currents in auditory neurons of mice lacking the channel subunit Kv1.1. J Physiol 548:1–20. CrossRef Medline

Brew HM, Gittelman JX, Silverstein RS, Hanks TD, Demas VP, Robinson LC, Robbins CA, McKee-Johnson J, Chiu SY, Messing A, Tempel BL (2007) Seizures and reduced life span in mice lacking the potassium channel subunit Kv1.2, but hypoexcitability and enlarged Kv1 currents in auditory neurons. J Neurophysiol 98:1501–1525. CrossRef Medline

Chen P, Dendorfer A, Finol-Urdaneta RK, Terlau H, Olivera BM (2010) Biochemical characterization of kappaM-RIIIJ, a Kv1.2 channel blocker: evaluation of cardioprotective effects of kappaM-conotoxins. J Biol Chem 285:14882–14889. CrossRef Medline

Crozier RA, Davis RL (2014) Unmasking of spiral ganglion neuron firing dynamics by membrane potential and neurotrophin-3. J Neurosci 34:9688–9702. CrossRef Medline

Devaux J, Alcaraz G, Grinspan J, Bennett V, Joho R, Crest M, Scherer SS (2003) Kv3.1b is a novel component of CNS nodes. J Neurosci 23:4509–4518. Medline

Dodson PD, Barker MC, Forsythe ID (2002) Two heteromeric Kv1 potassium channels differentially regulate action potential firing. J Neurosci 22:6953–6961. Medline

Fruman DA, Meyers RE, Cantley LC (1998) Phosphoinositide kinases. Annu Rev Biochem 67:481–507. CrossRef Medline

Gittelman JX, Tempel BL (2006) Kv1.1-containing channels are critical for temporal precision during spike initiation. J Neurophysiol 96:1203–1214. CrossRef Medline

Glowatzki E, Fuchs PA (2002) Transmitter release at the hair cell ribbon synapse. Nat Neurosci 5:147–154. CrossRef Medline

Grant L, Yi E, Glowatzki E (2010) Two modes of release shape the postsynaptic response at the inner hair cell ribbon synapse. J Neurosci 30:4210–4220. CrossRef Medline

Hossain WA, Antic SD, Yang Y, Rasband MN, Morest DK (2005) Where is the spike generator of the cochlear nerve? Voltage-gated sodium channels in the mouse cochlea. J Neurosci 25:6857–6868. CrossRef Medline

Jagger DJ, Housley GD (2002) A-type potassium currents dominate repolarisation of neonatal rat primary auditory neurones in situ. Neuroscience 109:169–182. CrossRef Medline

Jagger DJ, Housley GD (2003) Membrane properties of type II spiral ganglion neurones identified in a neonatal rat cochlear slice. J Physiol 552:525–533. CrossRef Medline

Jensen CS, Rasmussen HB, Misonou H (2011) Neuronal trafficking of voltage-gated potassium channels. Mol Cell Neurosci 48:288–297. CrossRef Medline

Johnston J, Postlethwaite M, Forsythe ID (2009) The impact of synaptic conductance on action potential waveform: evoking realistic action potentials with a simulated synaptic conductance. J Neurosci Methods 183:158–164. CrossRef Medline

Johnston J, Forsythe ID, Kopp-Scheinpflug C (2010) Going native: voltage-gated potassium channels controlling neuronal excitability. J Physiol 588:3187–3200. CrossRef Medline

Kruse M, Hille B (2013) The phosphoinositide sensitivity of the K(v) channel family. Channels (Austin) 7:530–536. CrossRef Medline

Kruse M, Hammond GR, Hille B (2012) Regulation of voltage-gated potassium channels by PI(4,5)P2. J Gen Physiol 140:189–205. CrossRef Medline

Liberman MC (1982) The cochlear frequency map for the cat: labeling auditory-nerve fibers of known characteristic frequency. J Acoust Soc Am 72:1441–1449. CrossRef Medline

Liu Q, Lee E, Davis RL (2014) Heterogeneous intrinsic excitability of murine spiral ganglion neurons is determined by Kv1 and HCN channels. Neuroscience 257:96–110. CrossRef Medline

Lv P, Wei D, Yamoah EN (2010) Kv7-type channel currents in spiral ganglion neurons: involvement in sensorineural hearing loss. J Biol Chem 285:34699–34707. CrossRef Medline

Lv P, Sihn CR, Wang W, Shen H, Kim HJ, Rocha-Sanchez SM, Yamoah EN (2012) Posthearing Ca(2+) currents and their roles in shaping the different modes of firing of spiral ganglion neurons. J Neurosci 32:16314–16330. CrossRef Medline

Lysakowski A, Gaboyard-Niay S, Calin-Jageman I, Chatlani S, Price SD, Eatock RA (2011) Molecular microdomains in a sensory terminal, the vestibular calyx ending. J Neurosci 31:10101–10114. CrossRef Medline

Manis PB, Marx SO (1991) Outward currents in isolated ventral cochlear nucleus neurons. J Neurosci 11:2865–2880. Medline

McGinley MJ, Oertel D (2006) Rate thresholds determine the precision of temporal integration in principal cells of the ventral cochlear nucleus. Hear Res 216:52–63. CrossRef Medline

Meyer AC, Frank T, Khimich D, Hoch G, Riedel D, Chapochnikov NM, Yarin YM, Harke B, Hell SW, Egner A, Moser T (2009) Tuning of synapse number, structure and function in the cochlea. Nat Neurosci 12:444–453. CrossRef Medline

Mi H, Deerinck TJ, Ellisman MH, Schwarz TL (1995) Differential distribution of closely related potassium channels in rat Schwann cells. J Neurosci 15:3761–3774. Medline

Mo ZL, Davis RL (1997) Endogenous firing patterns of murine spiral ganglion neurons. J Neurophysiol 77:1294–1305. Medline

Mo ZL, Adamson CL, Davis RL (2002) Dendrotoxin-sensitive K(+) currents contribute to accommodation in murine spiral ganglion neurons. J Physiol 542:763–778. CrossRef Medline

Moser T, Beutner D (2000) Kinetics of exocytosis and endocytosis at the cochlear inner hair cell afferent synapse of the mouse. Proc Natl Acad Sci U S A 97:883–888. CrossRef Medline

Nayagam BA, Muniak MA, Ryugo DK (2011) The spiral ganglion: connecting the peripheral and central auditory systems. Hear Res 278:2–20. CrossRef Medline

Nunoki K, Ishii K, Okada H, Yamagishi T, Murakoshi H, Taira N (1994) Hybrid potassium channels by tandem linkage of inactivating and noninactivating subunits. J Biol Chem 269:24138–24142. Medline

O'Leary SJ, Richardson RR, McDermott HJ (2009) Principles of design and biological approaches for improving the selectivity of cochlear implant electrodes. J Neural Eng 6:055002. CrossRef Medline

Pinyon JL, Tadros SF, Froud KE, Wong AC, Tompson IT, Crawford EN, Ko M, Morris R, Klugmann M, Housley GD (2014) Close-field electroporation gene delivery using the cochlear implant electrode array enhances the bionic ear. Sci Transl Med 6:233ra254. CrossRef Medline

Po S, Roberds S, Snyders DJ, Tamkun MM, Bennett PB (1993) Heteromultimeric assembly of human potassium channels: molecular basis of a transient outward current? Circ Res 72:1326–1336. CrossRef Medline

Rasband MN, Trimmer JS (2001) Developmental clustering of ion channels at and near the node of Ranvier. Dev Biol 236:5–16. CrossRef Medline

Rasband MN, Trimmer JS, Schwarz TL, Levinson SR, Ellisman MH, Schachner M, Shrager P (1998) Potassium channel distribution, clustering, and function in remyelinating rat axons. J Neurosci 18:36–47. Medline

Robbins J, Marsh SJ, Brown DA (2006) Probing the regulation of M (Kv7) potassium channels in intact neurons with membrane-targeted peptides. J Neurosci 26:7950–7961. CrossRef Medline

Rodriguez-Menchaca AA, Adney SK, Tang QY, Meng XY, Rosenhouse-Dantsker A, Cui M, Logothetis DE (2012) PIP2 controls voltage-sensor movement and pore opening of Kv channels through the S4-S5 linker. Proc Natl Acad Sci U S A 109:E2399-E2408. CrossRef Medline

Rutherford MA, Chapochnikov NM, Moser T (2012) Spike encoding of neurotransmitter release timing by spiral ganglion neurons of the cochlea. J Neurosci 32:4773–4789. CrossRef Medline

Schwarz DW, Puil E (1997) Firing properties of spherical bushy cells in the anteroventral cochlear nucleus of the gerbil. Hear Res 114:127–138. CrossRef Medline

Shnerson A, Pujol R (1981) Age-related changes in the C57BL/6J mouse cochlea: I. Physiological findings. Brain Res 254:65–75. CrossRef Medline

Siegel JH (1992) Spontaneous synaptic potentials from afferent terminals in the guinea pig cochlea. Hear Res 59:85–92. CrossRef Medline

Smith PH (1995) Structural and functional differences distinguish principal from nonprincipal cells in the guinea pig MSO slice. J Neurophysiol 73: 1653–1667. Medline

Suh BC, Hille B (2002) Recovery from muscarinic modulation of M current channels requires phosphatidylinositol 4,5-bisphosphate synthesis. Neuron 35:507–520. CrossRef Medline

Suh BC, Hille B (2008) PIP2 is a necessary cofactor for ion channel function: how and why? Annu Rev Biophys 37:175–195. CrossRef Medline

Szabó ZS, Harasztosi CS, Sziklai I, Szûcs G, Rusznak Z (2002) Ionic currents determining the membrane characteristics of type I spiral ganglion neurons of the guinea pig. Eur J Neurosci 16:1887–1895. CrossRef Medline

Wang H, Kunkel DD, Martin TM, Schwartzkroin PA, Tempel BL (1993) Heteromultimeric K^+ channels in terminal and juxtaparanodal regions of neurons. Nature 365:75–79. CrossRef Medline

Wang W, Kim HJ, Lv P, Tempel B, Yamoah EN (2013) Association of the Kv1 family of K^+ channels and their functional blueprint in the properties of auditory neurons as revealed by genetic and functional analyses. J Neurophysiol 110:1751–1764. CrossRef Medline

Warr WB, Boche JE (2003) Diversity of axonal ramifications belonging to single lateral and medial olivocochlear neurons. Exp Brain Res 153:499–513. CrossRef Medline

Werkman TR, Gustafson TA, Rogowski RS, Blaustein MP, Rogawski MA (1993) Tityustoxin-K alpha, a structurally novel and highly potent K^+ channel peptide toxin, interacts with the alpha-dendrotoxin binding site on the cloned Kv1.2 K^+ channel. Mol Pharmacol 44:430–436. Medline

Yano H, Nakanishi S, Kimura K, Hanai N, Saitoh Y, Fukui Y, Nonomura Y, Matsuda Y (1993) Inhibition of histamine secretion by wortmannin through the blockade of phosphatidylinositol 3-kinase in RBL-2H3 cells. J Biol Chem 268:25846–25856. Medline

Yi E, Roux I, Glowatzki E (2010) Dendritic HCN channels shape excitatory postsynaptic potentials at the inner hair cell afferent synapse in the mammalian cochlea. J Neurophysiol 103:2532–2543. CrossRef Medline